*Sedimentology* (1984) **31**, 195–211

# Sedimentology of the Minette oolitic ironstones of Luxembourg and Lorraine: a Jurassic subtidal sandwave complex

T. A. L. TEYSSEN*

*Geologisches Institut, Universität Bonn, Nussallee 8 5300 Bonn, Germany*

## ABSTRACT

The oolitic ironstones of the Minette were deposited during Toarcian/Aalenian times in a nearshore environment of the Paris Basin. The sedimentary sequence comprises up to 13 coarsening upward depositional cycles. The development of the cycles and different facies types are described. The iron ooids accumulated in a subtidal environment under the effects of tidal currents. Sand waves, which form an important part of the Minette sediments, were deposited under both time-velocity symmetrical and time-velocity asymmetrical tides. From the study of their internal structures the time-velocity patterns of the currents, current speeds (up to 0·9m $s^{-1}$) and net transport rates have been estimated (29 g $m^{-1}$ $s^{-1}$ in the case of large-scale sand waves controlled by time-velocity symmetrical tides). Sand wave heights and calculated near-bed current speeds suggest a mesotidal regime. Sedimentary facies include large-scale sand waves, subtidal shoals with channels and an offshore muddy shelf. Conclusions as to bathymetry are drawn from ichnofaunal associations and from the study of wave ripple marks. Finally a depositional model of the Minette iron formation is proposed which may be applicable to other oolitic ironstones.

## INTRODUCTION

The Minette oolitic ironstones are the type ore deposit of the Phanerozoic shallow marine, oolitic Minette- or Clinton-type Iron Formations. Whereas much work has been done on the mineralogy and geochemistry (Cayeux, 1922, Taylor, 1949, Hallimond, 1951, Kimberley, 1979, James & van Houten, 1979 and many others) and diagenesis (Bubenicek, 1971, 1983), less emphasis has been placed on the sedimentology of these ironstone deposits (Bubenicek, 1964; van Houten & Karasek, 1981; Hallam, 1966; Dimroth, 1977; Bhattacharyya, 1980). Investigations on the genesis of the iron ooids of the Minette ironstones have recently been conducted (Siehl & Thein, 1978). The aim of this study is to reconstruct the depositional processes which formed the ironstones.

The Minette oolitic ironstones were deposited in late Toarcian and early Aalenian times in a NE-striking marginal trough of the Paris Basin (Fig. 1, cf. also Megnien, 1980). There were two basins of ironstone deposition, the larger Briey Basin (Fig. 2) in Luxembourg and northern Lorraine, and the smaller Nancy Basin in central Lorraine. This study deals with the Briey Basin.

The Briey Basin was divided into two sub-basins, Esch-Ottange and Differdange-Longwy (Fig. 2). In the basin of Differdange-Longwy the deposition of ironstones began earlier, but also ended earlier than in the basin of Esch-Ottange (cf. Thein, 1975; Achilles & Schulz, 1980). The two sub-basins were separated by the Audun-le-Tiche fault which was active during sedimentation (Lucius, 1945), as were most of the other NE-striking faults (Achilles & Schulz, 1980).

The Minette sediments were deposited under the influence of tidal currents, as can be concluded from sedimentary structures as internal structures of sand waves, bipolar cross-stratification and bipolar orientation of belemnites, and occasional channel fill deposits. The conclusions on the tidal origin of the ironstones will be outlined in detail in the following sections.

* Present address: Koninklijke/Shell Exploratie en Produktie Laboratorium, Volmerlaan 6, 2288 GD Rijswijk ZH, The Netherlands.

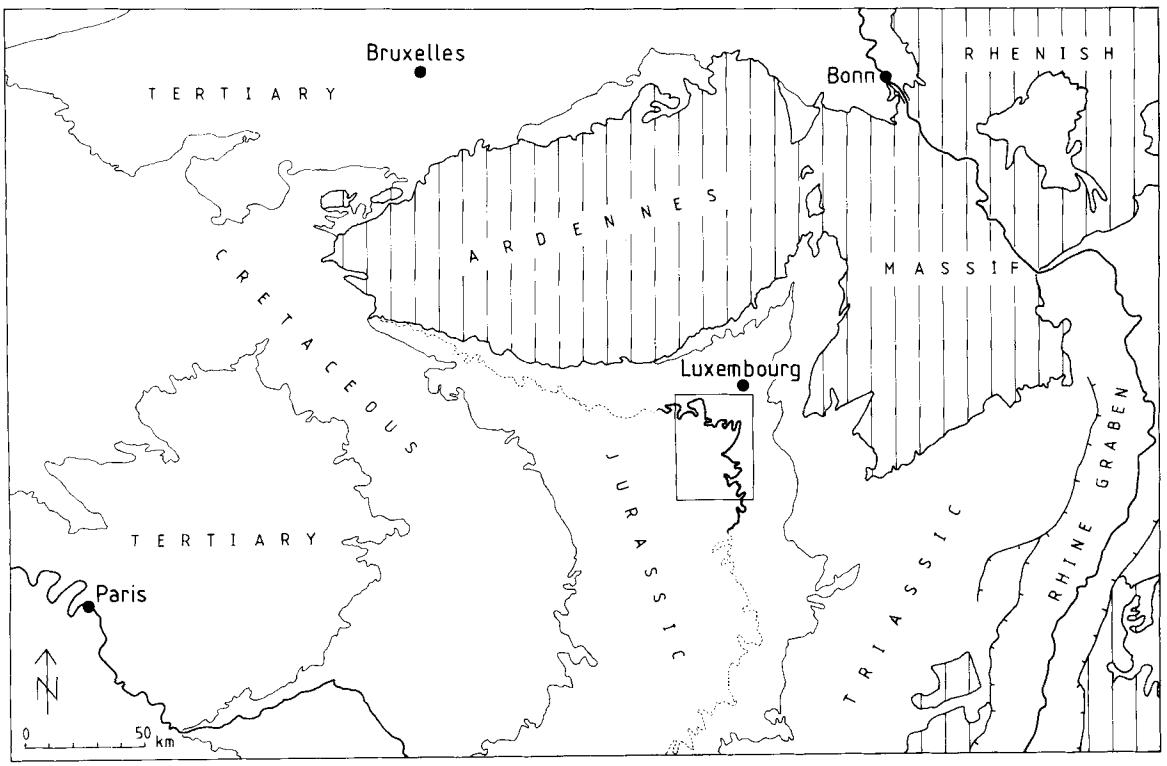


**Fig. 1.** Area of investigation in the north-eastern part of the Paris Basin. Dashed line is the outcrop of the Toarcian–Aalenian boundary. The position of the Basin of Briey south of Luxembourg is outlined.

## LITHOSTRATIGRAPHY AND FACIES

The sedimentary sequence has a cyclic pattern (Bubenicek, 1964; Thein, 1975; Siehl & Thein, 1978; Achilles & Schulz, 1980) which is the basis of the stratigraphical subdivision. Up to 13 cycles are present. A cycle develops from a muddy facies (*Zwischenmittelfazies* in the German, *Intercalcaire* in the French literature) to a transitional facies and an ironstone facies (*Lagerfazies*, *Couche*). The cycle generally ends with a coquina bed (Fig. 3). Within these coarsening upward cycles there is a general increase in grain size, ooid content, bioclast content, and probable current strength, and a decrease in bioturbation (Fig. 3).

The muddy facies is composed of fine grained, silty and muddy sediments which are poor in iron ooids. The sedimentary structures are linsen- and flaser-bedding, but in most cases the bioturbation has more or less completely destroyed the primary structures. Trace fossils comprise *Rhizocorallium jenense*, *R. irregulare*, *Planolites beverleyensis*, *Palaeophycus tubularis*, *Phycodes*, *Teichichnus*, *Dendrotichnium alternans* and *Olivellites*. Bivalves are commonly found in living position. Belemnites show a bipolar orientation.

In the transitional facies the size of cross-sets increases but ripple cross-lamination and small-scale cross-bedding predominate. The iron ooid content also increases and bioturbation is less pronounced.

The ironstone facies is composed of iron rich rocks containing limonitic and chamositic ooids. Limonitic ooids are composed of goethite (Braun, 1964; Thein, 1975), the latter containing seven Å-bertierine and 14 Å-chamosite (Orcel, Hénin & Caillère, 1949; Millot, 1970; cf. also Brindley *et al.*, 1968; Odin & Matter, 1981). The ooids generally have a more or less elliptical shape; the cores are of quartz or of fragments of iron ooids or iron crusts and rarely of echinoderm fragments (Siehl & Thein, 1978). The median grain size of the ooids varies between 0·2 and 0·5 mm. Quartz is of sand and silt grain size with angular to subrounded grains of silt fraction and well rounded and sorted grains of sand size. Bioclasts and whole fossils (bivalves and belemnites, rarely ammonites) are

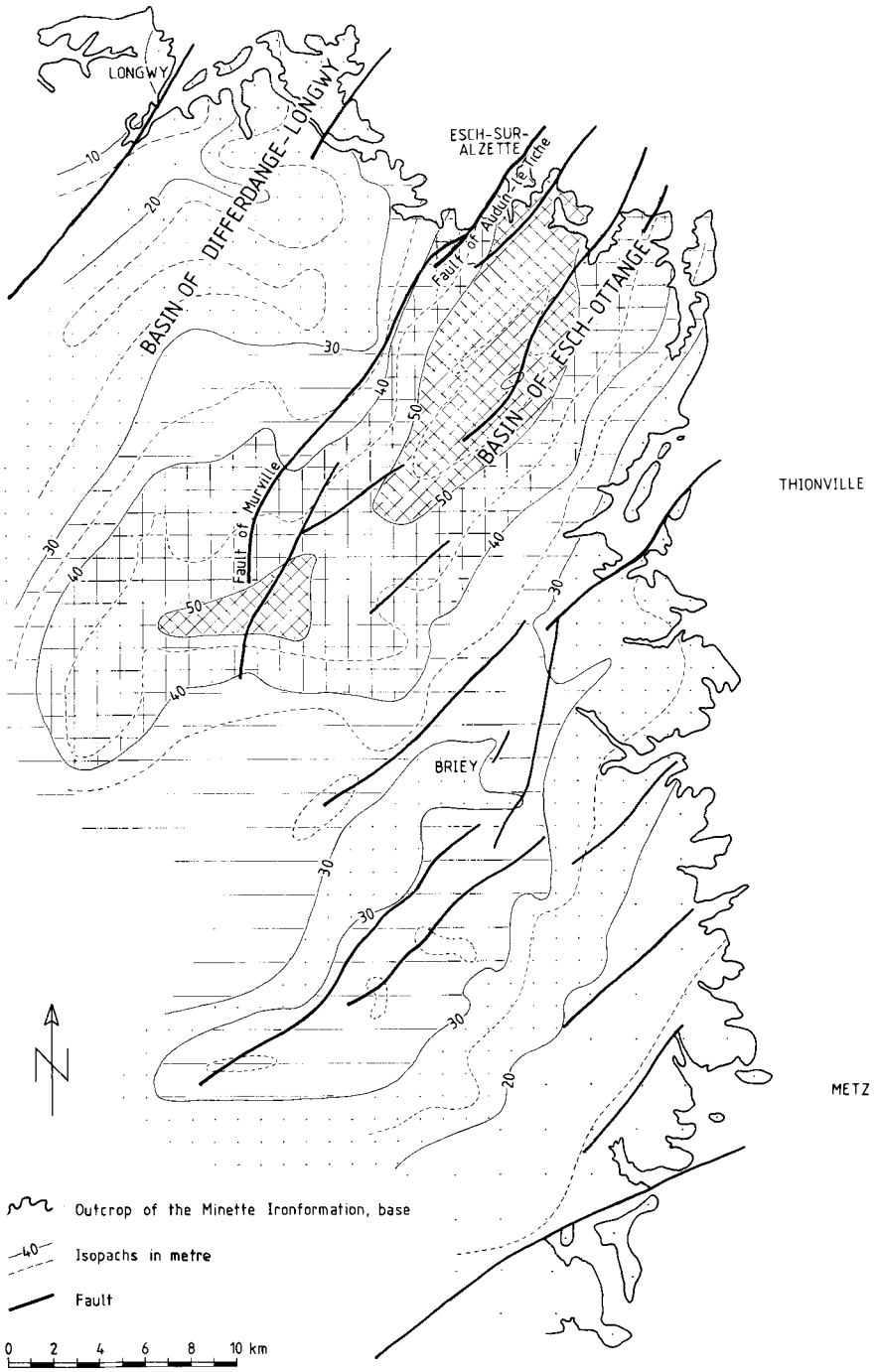


**Fig. 2.** Thickness of the Minette Iron Formation of the Basin of Briey after IRSID (1967), faults after Lucius (1945). The fault of Audun-le-Tiche separates the subbasin of Esch-Ottange from the subbasin of Differdange-Longwy.

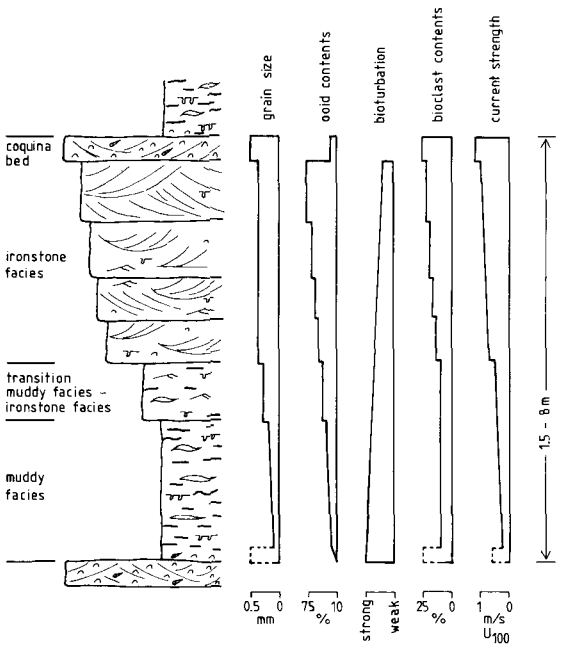


**Fig. 3.** Schematic sketch of a depositional cycle of the Minette deposits. The sequence leads from a muddy facies to a transitional facies and the ironstone facies with an overlying coquina bed. Grain size, contents of iron ooids and of bioclasts and current strength increase; the bioturbation decreases. Scales give orders of magnitude. See text for further explanation.

abundant. Cementation of the ironstones is partly calcitic (neomorphic sparite), partly sideritic-chloritic (Bubenicek, 1983). The ooid sands are well sorted and locally very well sorted.

The sedimentary structures of the ironstone facies are small- to medium-scale cross-stratification due to bipolar current directions and herringbone-structures. Wave and current ripples and sand waves are abundant. The lebensspuren comprise *Spongeliomorpha nodosa*, *Arenicolites variabilis*, *Skolithos* and escape traces.

The asymmetrical cycles can easily be discerned in the outcrop. The facies of the lower part of the Minette Formation are generally as described above. In the upper part of the formation the differences between muddy facies and ironstone facies are less pronounced with respect to both petrography and sedimentary structures. Locally, several coquina beds can be found within a cycle. The occurrence of these coquinas and the minor differences between muddy facies and ironstone facies have been explained by a shallowing of water depth in the upper part of the Iron Formation (Achilles & Schulz, 1980; Teyssen, 1983a). Some fining upward sequences within a coarsening upward cycle, found in the upper part of the formation, are considered to represent filling up and silting up of channels.

A cyclic development as described above is also a typical feature of other Minette-type Iron Formations such as those of England (Hallam & Bradshaw, 1979) or especially of the Devonian Shatti Formation of Libya (van Houten & Karasek, 1981) and of the Cretaceous Nubia Formation of Egypt (Bhattacharyya, 1980). In these examples, as well as in the Minette of Luxembourg and France (Bubenicek, 1971; Siehl & Thein, 1978; Megnien, 1980), the muddy facies has been thought to represent offshore shelf muds and the ironstone facies to represent subtidal bars. In that model one regression would have produced one cycle and each regression was followed by a transgression. Although many ironstone sequences might well reflect sea-level changes (e.g. those of England, see Hallam & Bradshaw, 1979), there is no explanation in detail for an external control of the very regular cyclic pattern of sedimentation. This paper will propose an autocyclic depositional model of the Minette Iron Formation which avoids the difficulties of some of the other models.

## SAND WAVE EVOLUTION IN THE MINETTE

The bipolar cross-stratification suggests a tidal control of sedimentation (see Thein, 1975). The need for substantiation of the tidal control led to the recognition and investigation of sand waves which form a considerable portion of the Minette sediments. Different types of sand waves (*sensu* Allen, 1980, implying evolution under true reversing currents) in the Minette, with particular internal structures, reflect different tidal systems. Two main types of tidal systems need to be considered (cf. Allen, 1980):

(1) Time-velocity asymmetrical tides result from superimposition of a strictly periodic component $U_p(t)$ on a steady component $U_s$, $U_s$ not being small in comparison with the peak value of $U_p(t)$. In this case the sediment transport rate due to the dominant current considerably exceeds the rate due to the subordinate current (Allen, 1980, fig. 4; Allen, 1982; Heath, 1981; Teyssen, 1984).

(2) Time-velocity symmetrical tides, on the other hand, result from superimposition of a periodic flow $U_p(t)$ on a steady component $U_s$, but $U_s$ being small in

comparison with the peak value of $U_p(t)$ (Allen, 1980). In this case the transport rates of the two reversing currents are more or less comparable.

### Sand waves controlled by time-velocity symmetrical tides

Sand waves of this category have been studied in many recent examples, such as in the North Sea (Houbolt, 1968; Kenyon *et al.*, 1981), the Jade estuary of northern Germany (Reineck, 1963) and the Yellow Sea (Klein *et al.*, 1982). Although Allen (1980) gave some very useful theoretical considerations, no satisfactory example of ancient sand waves clearly laid down under control of time-velocity symmetrical tides has so far been recognized and described. The Minette iron formation, however, displays some very well-developed examples. They can best be studied in the Prinzenberg outcrop 2 km to the north of Differdange/Luxembourg (coordinates 58800 67350).

The sand waves show the following diagnostic features. The top of the sand wave (and of the respective depositional cycle of the Minette) is a sharp sedimentary discordance (Fig. 4A). The foresets of

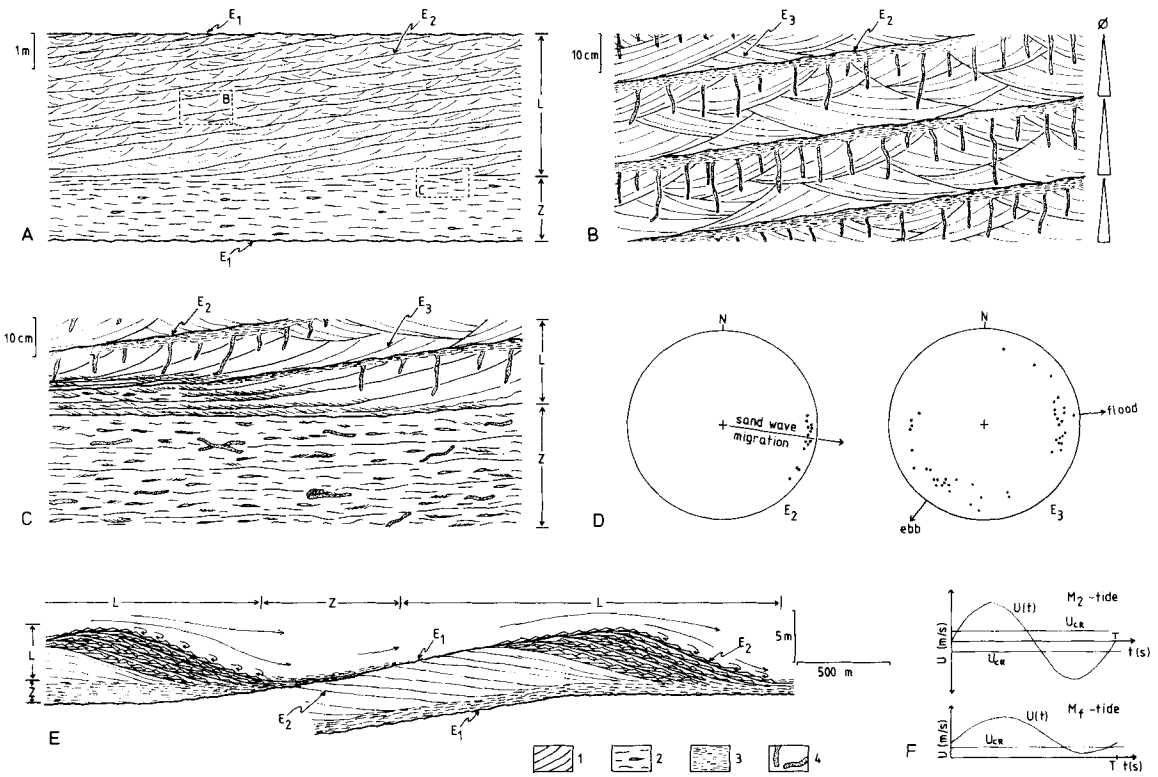


**Fig. 4.** Internal structure and model of sand wave evolution due to time-velocity symmetrical tides, Prinzenberg outcrop. L, ironstone facies; Z, muddy facies; $E_1$, first-order bedding planes; $E_2$, second-order bedding planes; $E_3$, third-order bedding planes; 1, cross-bedding; 2, linsen- and flaser-bedding; 3, silt- and mudstone, 4, bioturbation.

(A) General view of a sand wave of one depositional cycle, large-scale, low-angle foreset-beds (L) and flat lying bottomsets (Z).

(B) Detail from the foresets, beds with small-scale, bipolar cross-sets; cover of silt- and mudstone; at the right hand margin indication of grain-size tendency within a bed.

(C) Detail from the transition of the foresets into the bottomsets.

(D) Equal area projection of poles to cross-bed planes from a sand wave of the Lower Calcareous Cycle at the Prinzenberg locality; left: second-order bedding planes indicating the direction of migration of the sand wave; right: third-order bedding planes with bipolar directional distribution indicating local ebb and flood palaeoflow directions.

(E) Model of sand wave evolution.

(F) Time-velocity pattern of the governing partial tides, note the different period duration of the $M_2$ tide ($\sim$12 hr) and of the $M_f$ tide ($\sim$14 days).

the sand wave are composed of complex, low-angle dipping beds, which will here be called 'foreset-beds', not to be confused with 'foresets bundles' (Boersma, 1969; Visser, 1980) of sand waves under control of time-velocity asymmetrical tides. The foreset-beds can be traced from the discordance at the top through the ironstone facies (upper part of a cycle) into the muddy facies (lower part of the cycle), such that isochronous lines cut the boundary between ironstone facies and muddy facies. The thickness of individual beds is of the order of 0·2 m. Within the foreset-beds, small scale, bipolar cross-stratification can be identified (Fig. 4B). The beds are bioturbated, with vertical burrows which penetrate downward from the top of the bed. The muddy facies in the lower part of the sand wave consists of bioturbated linsen-bedded sediments. The height of a sand wave, and therefore of a sedimentary cycle, was in excess of 6 m.

Following Allen (1980) three different bedding planes can be identified (Figs 4 and 8): first-order bedding planes ($E_1$) are the discordances between sand waves, that is the surface upon which the sand wave migrated (Fig. 4A, E). Second-order bedding planes ($E_2$) are the interfaces between the low-angle foreset-beds (Fig. 4A, B). These planes correspond to the steeper lee-slope of the sand wave (Fig. 4E). Third-order bedding planes ($E_3$) are due to the small-scale cross-stratification within the beds (Fig. 4B).

The crest lines of the sand waves were straight or slightly curved as shown by reconstruction from the Prinzenberg exposure (Fig. 5).

The ironstone facies originated as foreset-bed sediments on the lee-slope during migration of the sand wave. Reversing currents of nearly equal strength (but not exactly equal strength, see below) caused reversing bedload transport of sand upon the slope as small-scale cross-sets (Fig. 4B, E). The muddy facies originated between the sand wave crests as bottomset deposits of the sand wave.

Deposition and erosion of cross-sets within the foreset-beds, due to the alternating currents, ceased around neap tides. The final cross-sets of each spring tide period, with its traces of suspension feeders, were thus preserved. During neap tide periods the silt and mud cover of the beds was laid down (Fig. 4B).

The very regular development of a sand wave with its foreset-beds cannot be explained by considering the 12·4 hr $M_2$ tide only as Allen (1980) has done in his theoretical approach. This component determines the small-scale trough cross-bedding. The very regular development of the foreset beds seems to have been externally controlled also. But since there is no periodic

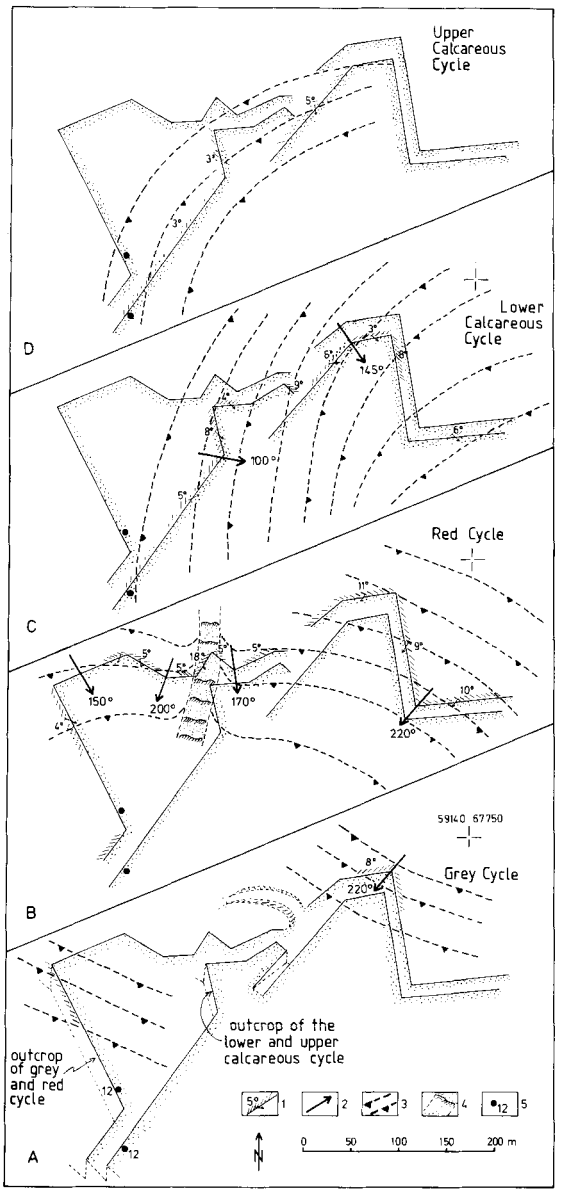


**Fig. 5.** Map of sand wave crest-lines observed in the different depositional cycles of the Prinzenberg exposure (from bottom to top): A, Grey Cycle; B, Red Cycle; C, Lower Calcareous Cycle; D, Upper Calcareous Cycle. 1, Outcrop wall with indication of the apparent dip of second-order bedding planes ($E_2$). 2, Local direction of migration of the sand wave. 3, Crest-line of the sand wave at different moments. 4, Cut of the sand wave of the Red Cycle by a subtidal channel, within this channel smaller-scale sand waves were formed which were controlled by time-velocity asymmetrical tides due to channelized flow. 5, Site and number of a stratigraphical section.

variation in foreset-bed thickness over some hundred metres of outcrop length (which comprises more than 200 beds), the partial tide which gave rise to the formation of foreset beds must itself be controlled by another longer-period partial tide. On the other hand the partial tide under consideration must cause a component of tide force which is strong enough to be well reflected in the geological record. The only partial tide which fits these requirements is the 327·9 hr $M_f$ tide. The development of the sand wave is therefore suggested to result from the effects of both the $M_2$ tide and the $M_f$ tide (Fig. 4F). In attributing a foreset-bed to the 327·9 hr $M_f$ tide the net sediment transport rate (averaged over a lunar cycle) of the Prinzenberg example can be estimated as 28·9 g $m^{-1}$ $s^{-1}$ (sand wave height 6 m, thickness of foreset beds 0·2 m, dip angle of beds 7°, sediment density 3·6 g $cm^{-3}$ calculated from the contents of iron ooids, quartz and bioclasts of the rocks. The primary density might have been smaller because of a probable greater porosity of the iron ooids during deposition.)

The time-velocity pattern of the governing currents can also be reconstructed. The local ebb and flood current directions can be determined from cross-bedding measurements within the foreset beds (Fig. 4D). By measuring the orientation of the foreset beds, the direction of migration of the sand wave can be determined (Fig. 4D). The slope of the foresets was steepened by the flood current and flattened by the ebb. That the slightly dominating current was the flood can be concluded from the palaeogeographical reconstruction (Teyssen, 1983a). Since the directions of flood, ebb, and that of migration are related to each other, the strength of the two currents must be such that the sand wave develops in equilibrium with the governing forces. This equilibrium condition allows the estimation of the ratio of ebb and flood sediment transport rates $J_1$ and $J_2$ applying basic physical concepts (Fig. 6A). Unfortunately that ratio cannot easily be transformed to the more important ratio of peak velocities $U_1$ and $U_2$ because there are many possible solutions of the required ratio of peak velocities. Figure 6(B) gives two solutions having been suitably but arbitrarily chosen from the set of possible solutions. These two are mathematically equivalent, chosen such that both equally have the required ratio of transport rates and equal threshold velocities for bedload sediment entrainment (being a function of grain size and grain density), but they then necessarily have different ratios of peak speeds (1·8 and 1·64 respectively) and different high steady flow components (0·285 and 0·17 respectively). The ratio of peak speeds obviously varies with the value of the greater peak velocity (Fig. 6C). Since very high near-bed velocities seem not to be probable because of the small-scale cross-sets, a ratio of peak velocities of about 1·5 seems to be acceptable (Fig. 6C). In adopting this approach one can also calculate Allen's (1980) velocity symmetry index $V_2$ (as 0·2) and velocity strength index $V_1$ (as 1·5) for the fossil example (Fig. 6C). The plausibility of these figures can be deduced by referring to Allen's (1980, fig. 8) regime diagram for sand waves which has been set up for a value of $(U_{p\max} + U_s)$ being slightly different from that suitable for the Prinzenberg sand waves. The Prinzenberg example must then be attributed to class V (cf. Fig. 8) which was also suggested from inspection of the internal structures.

## Sand waves controlled by time-velocity asymmetrical tides

Sand waves controlled by time-velocity asymmetrical tides have in recent years been the focus of discussion, particularly with respect to internal structures, stability and dynamics (Nio, 1976; Visser, 1980; Boersma & Terwindt, 1981; Allen, 1982; Langhorne, 1982; Allen & Homewood, 1984; Teyssen, 1983b, 1984). These sand waves have been studied in recent and fossil examples from siliciclastic rocks.

Sand waves controlled by time-velocity asymmetrical tides with bundle structure occur widely in the Minette sediments. In all cases these sand waves form part of the ironstone facies at the upper part of a depositional cycle. Evolution of these sand waves is not directly related to the sedimentation of the underlying muddy facies, in contrast to the situation in sand waves under control of time-velocity symmetrical tides.

One of the best examples of a sand wave controlled by time-velocity asymmetrical tides is in the outcrop south of Maison Schneider between Rédange and Hussigny-Godbrange (France) (coordinates 60130 62030). Figure 7 (A) displays the internal structures of a part of the sand wave. The tidal bundles, which are attributed to the ebb current because of palaeogeographical constraints (Fig. 13), are separated by coupled mud layers. Thin layers or lenses of flood sands were laid down between the slack water mud drapes. Ripples due to ebb-current backflow, and flood current upslope flow can be recognized on the mud layers. The internal structures are comparable to those observed by Visser (1980) and Allen (1982) in

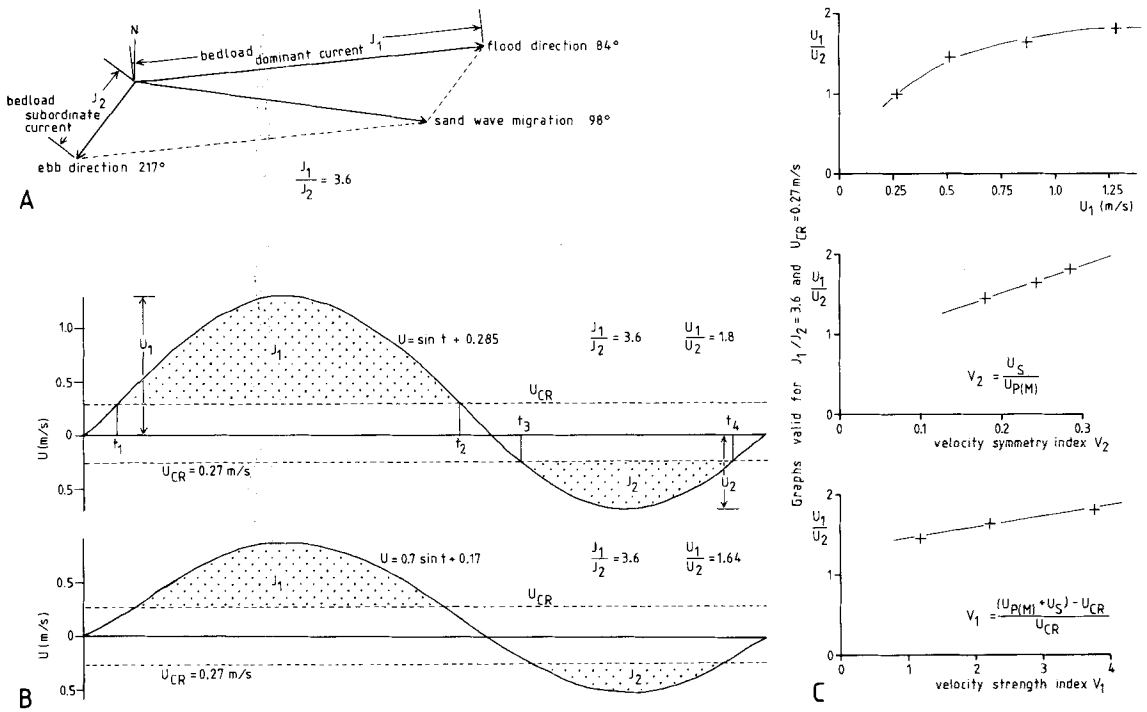


**Fig. 6.** Estimation of the time-velocity pattern of the tidal currents effective during deposition of the sand wave of the Lower Calcareous Cycle of the Prinzenberg outcrop. Indices $V_1$ and $V_2$ after Allen (1980). (A) Estimation of the ratio of sediment transport rates $J_1$ (flood) and $J_2$ (ebb) from tidal current directions and direction of migration of the sand wave. Evolution of the slope of the sand wave (direction of migration) is in equilibrium with maximum velocities and transport rates of the respective current stages. The slope is steepened in flood direction and again flattened in ebb direction. The indicated transport rates $J_1$ and $J_2$ cause transport of a sediment unit volume with the direction of migration of the sand wave. (B) Different solutions of the ratio $U_1/U_2$ of maximum tidal velocities with equal ratios of transport rates $J_1/J_2$, but different maximum flood velocities $U_1$ and different magnitudes of steady velocity component (0·285 and 0·17 respectively). The threshold velocity for bedload sediment entrainment is 0·27 m $s^{-1}$ in both cases. (C) Variation of the ratio of maximum tidal velocities $U_1/U_2$ with $U_1$ (top). Variation of the velocity symmetry index $V_2$ and of the velocity strength index $V_1$ with $U_1/U_2$ (bottom).

pure siliciclastic sand waves. Reactivation surfaces of class B (after de Mowbray & Visser, 1982) are developed. The sand wave has a preserved height of 1·5 m, but it seems to be truncated at the top. Considering this and the compaction of the carbonate-rich rocks an original height of at least 2 m is probable.

Dominant and subordinate current sands can also be distinguished from the grain size (Fig. 7B), the median of the ebb sands (dominant current stage) is about one phi unit coarser than that of the flood sands (subordinate current). The sorting of ebb and flood sand is comparable (Fig. 7D). Ebb and flood sands are different not only in grain size but also in composition (Fig. 7C). The ebb sediments contain mainly coarse, well-sorted iron ooids (72%) and a low amount of badly sorted quartz grains. In the flood sands the amount of quartz largely exceeds that of iron ooids (29%). Both the medians of quartz and iron ooids are smaller in flood than in ebb sediments. The sorting of quartz is much better in the flood sands. One may conclude that the less effective flood current caused a grain-selective transport of the sediments having been transported to the front of the sand wave by the previous ebb current. The flood ripples were mainly built up of the quartz grains of lesser density, sediment entrainment of the denser iron ooids was possible only to a limited extent. Some strange attributes of the grain-size distributions are that there are fewer coarse, well-rounded quartz grains which fit with their equivalent hydraulic diameter to the iron ooids, but there is more fine-grained, angular quartz. The coarse, probably denser ooids and fine, light

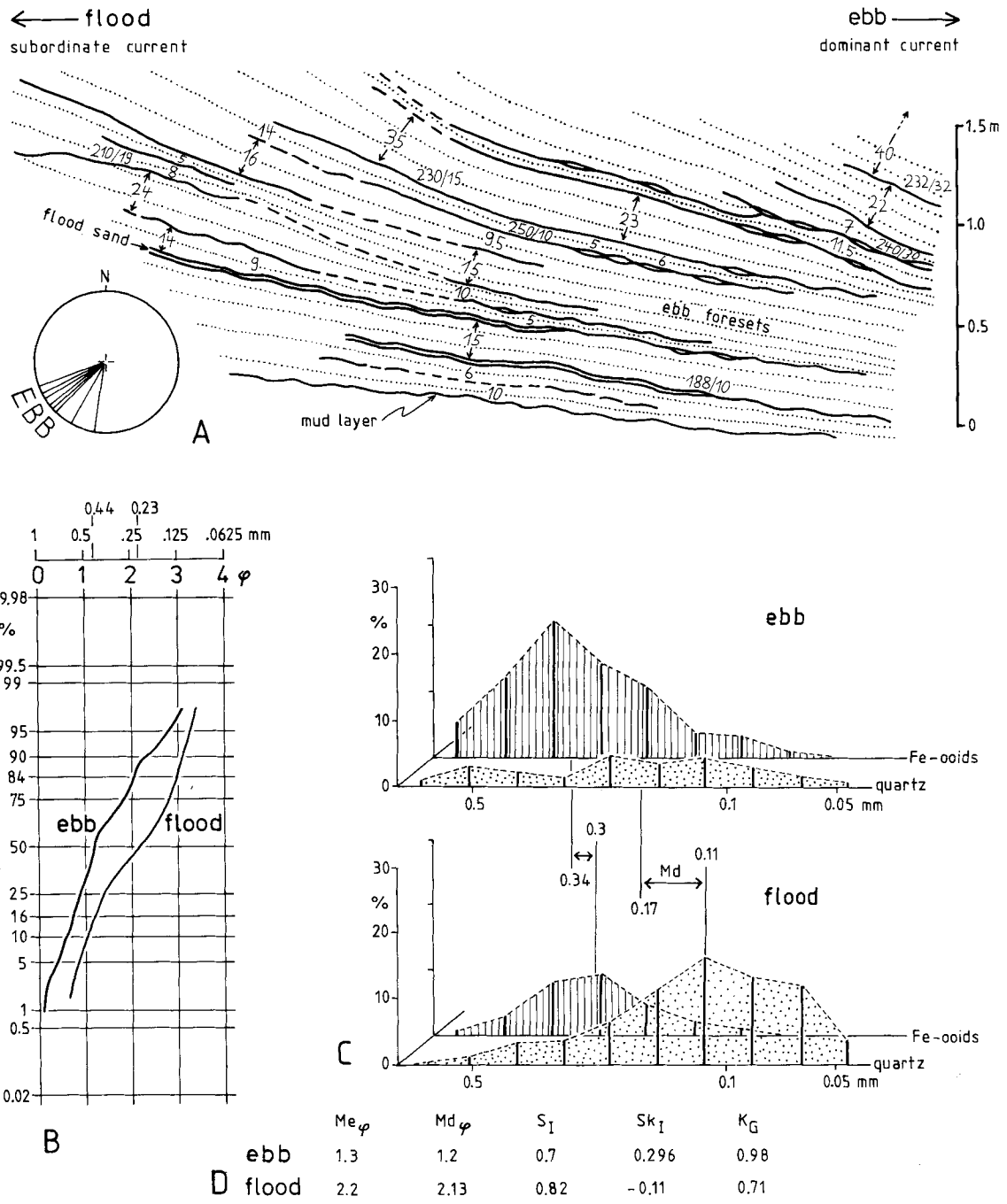


**Fig. 7.** Internal structure and grain size of a sand wave from the Red Cycle, south of Maison Schneider. (A) Sketch of the internal structure, the figures indicate thickness of tidal bundles and azimuth of dip/dip angle of the foresets. Diagram of palaeocurrent directions at the left margin. (B) Grain-size distribution of ebb and flood sands plotted in probability net. The distributions have been obtained from thin sections, the corpuscle effect was compensated by a Monte Carlo simulation (cf. Teyssen, 1983a). (C) Grain-size distributions of the subpopulations of iron ooids and quartz grains of the ebb and flood sediments (cf. text). (D) Folk & Ward parameters of the grain-size distributions of ebb and flood sediments.

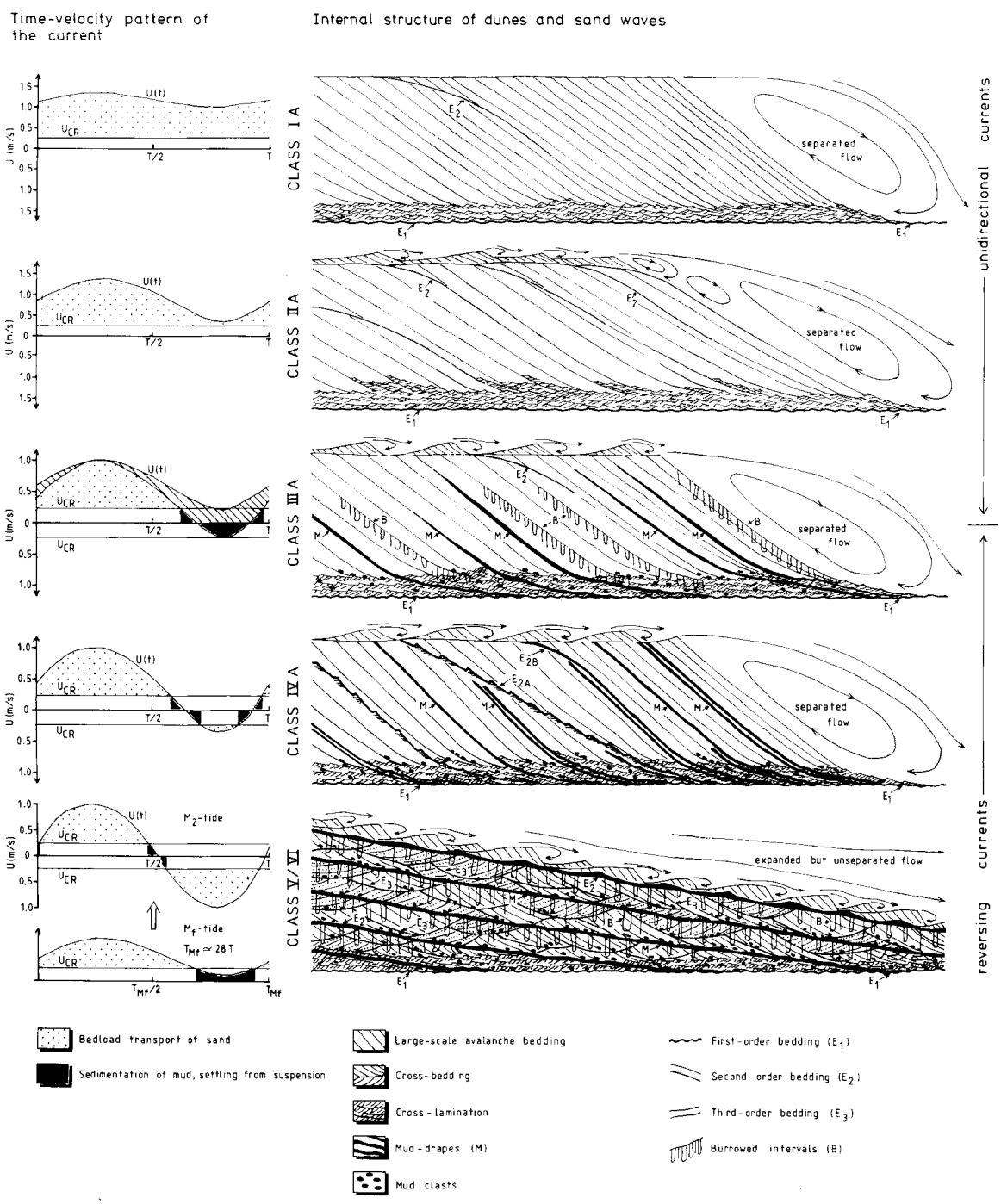


**Fig. 8.** Model of the internal structure of sand waves (right hand column) due to different time-velocity patterns of tidal currents (left hand column), redrawn and modified after Allen (1980). Internal structures and reactivation surfaces of class IV sand wave with reference to de Mowbray & Visser (1982), the classes V and VI of Allen (1980) have been combined.

quartz grains are not hydraulically equivalent in joint bedload transport. The reasons for this association, which is found in most Minette sediments and also in the Cretaceous Nubia deposits (Bhattacharyya, 1980, p. 21), and which suggests immature sediments with joint transport over only short distances, remain uncertain at present.

Estimation of the palaeotidal near bed ebb peak velocity effective during evolution of the described sand wave can be done using a kinematic model (Teyssen, 1984). This leads to a value of 0·9 m $s^{-1}$. Estimations using parameters of other sand waves from the same depositional cycle are of the same order. The relatively high palaeotidal flow velocities and heights of both types of sand waves would most probably fit to the assumption of a mesotidal regime (Hammond & Heathershaw, 1981; Teyssen, 1983a).

Sand waves as described above are very common in the Minette sediments, but sand waves with a different development can also be found. Some sand waves have bundles not separated by mud drapes. The bundle interfaces can nevertheless be clearly identified, because a fining upward tendency within the bundles gave rise to different cementation and later to different carbonate leaching. Mud drapes may not have been formed because of flow velocities being too high over the whole tidal cycle for settlement of mud from suspension (see Allen, 1982, for further discussion of drape suppression). Different evolution of mud drapes suggests different shapes of tidal current ellipses of rotary tides (Allen, 1982, fig. 13). Measurements of the thickness of tidal bundles show 'thin-thick'-alternations (cf. Teyssen, 1984) which suggest a semidiurnal tidal system (Visser & de Boer, 1982). Figure 8 gives a general model of sand wave internal structures due to different time-velocity patterns of the currents, which summarizes the observations made in the Minette.

## TRANSPORT DIRECTIONS

Tide-controlled sedimentation of the Minette Iron Formation was initially deduced from cross-bedding measurements. Measurements have been taken in the outcrop zone between Longwy (France) and Dudelange (Luxembourg) as well as in the subsurface in mines in France. Figure 9 gives a cumulative diagram of cross-bedding measurements in the Minette clearly displaying bipolar current directions. The bipolarity appears on cumulative diagrams of measurements of the separate depositional cycles, as well as in the

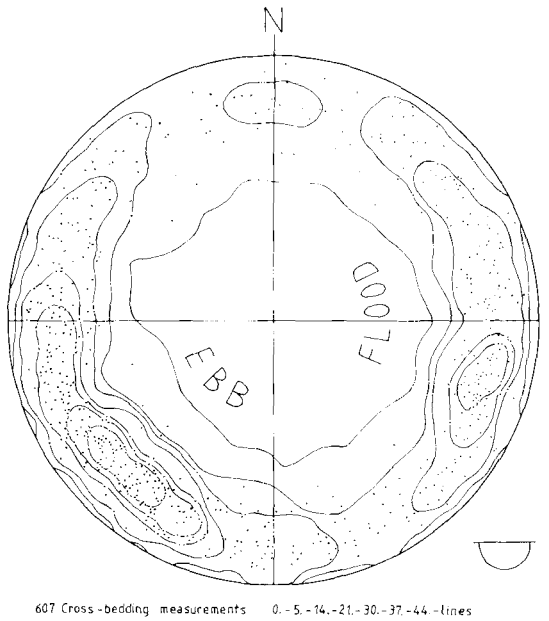


**Fig. 9.** Equal area projection of cross-bedding measurements from the Minette Iron Formation. Note the bipolarity of currents, ebb currents to the SW, flood currents to the east.

distributions from individual sites (Thein, 1975, appendix 4; Teyssen, 1983a). The flow pattern does not change significantly among the depositional cycles of the Formation (Teyssen, 1983a). The data from the individual measurement sites have been used for a vector trend surface analysis after Fox (1967) (cf. also Shakesby, 1981) to prepare maps displaying continuous flow pattern of ebb and flood currents (Fig. 10). The maps show flood currents to the NE and east and ebb currents to the SW and west. East and NE directions have been attributed to the flood because the Ardennes and Rhenish Massifs were probably emergent during deposition of the Minette (Fig. 13; Megnien, 1980, vol. I, fig. 4.10, 16.3; Ziegler, 1982, encl. 18). The ebb was generally the dominant current as shown by observations on many sand waves and by most of the directional distributions at individual measurement sites. Thus the ebb currents coincide with the net sediment transport directions, which is in accordance with the thickness distribution of the formation (Fig. 2). The results obtained here (Figs 9, 10 and 13) contradict the palaeogeographical conception of IRSID (Institut de Recherche de la Siderurgie, 1967). The different transport directions to the NE and SW were not restricted to geographically separated zones of marine and fresh-brackish water as

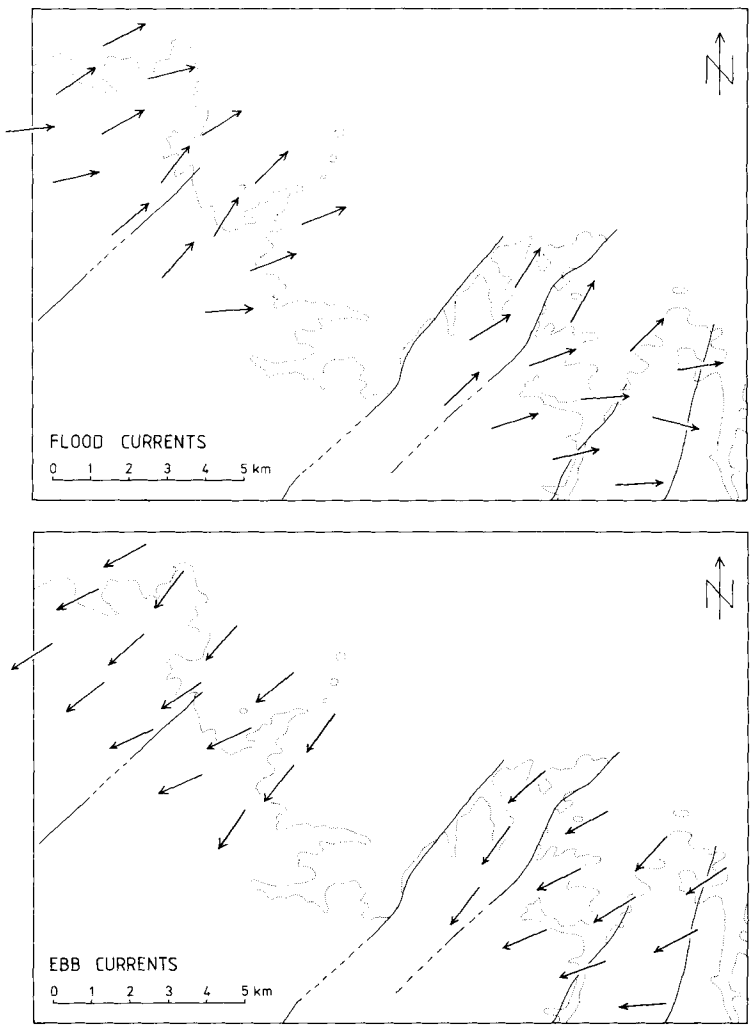


**Fig. 10.** Maps of flood and ebb palaeocurrents of the outcrop zone of the Minette evaluated from a trend surface analysis after Fox (1967), the trend being a sum of linear, quadratic and cubic surfaces.

stated in the IRSID atlas (1967), but nearly every measurement site shows interfingering of cross-sets due to both ebb and flood currents. Neither are there any palaeontological hints for brackish or fresh water as proposed by IRSID (1967). Sedimentary structures, fauna and trace fossils suggest a fully marine environment throughout the whole extent of the Minette Iron Formation.

## DEPOSITIONAL MODEL OF THE MINETTE

On the basis of the results presented above a depositional model of the Minette can be established both for vertical build-up and local palaeogeography (Figs 12 and 13).

It has been shown above that in the case of sand waves controlled by time-velocity symmetrical tides the facies types of one depositional cycle (muddy facies and ironstone facies) were formed under a continuous sedimentary process, the migration of a sand wave. In the Prinzenberg outcrop four sand waves have built up the sedimentary pile (Fig. 5) by overriding each other. Thus the cyclic sequence can be explained without assuming any transgression.

Sand waves migrated in a geological frame of a slowly prograding shoreline.

This explanation holds for a major part of the Minette sediments, but it does not apply to sand waves controlled by time-velocity asymmetrical tides found in the ironstone facies of a cycle. The deposition of that sand wave category is not related to the deposition of the muddy facies of the respective cycle. The sand waves are replaced laterally by deposits showing bipolar, small-scale, mostly trough cross-stratification, deposits which can be interpreted as (probably subtidal) shoals. The sand waves may have formed at the margins of those shoals or within subtidal channels. Channelized flow is in accordance with the relatively high subtidal flow velocities. The muddy facies is now to be interpreted either as intertidal muddy flats or as deeper water mud flats seaward in front of the shoals. The latter has already been assumed by Siehl & Thein (1978) and suggests prograding or shoal advance over a more distal muddy facies as also proposed in the model of van Houten & Bhattacharyya (1982). The problem can be solved from two independent lines of reasoning.

The first evidence comes from the bioturbation, which is different in the coarse grained shoal deposits and in the muddy facies. Figure 11 shows the ichnofaunal associations of the facies types together with their bathymetric ranges. Although conclusions as to precise bathymetry from trace fossils are not possible, an estimate of relative bathymetric differences between the muddy facies and the ironstone facies is given in Fig. 11 by comparison with other Jurassic trace fossil associations (Fürsich, 1974, 1975, 1976, 1977, 1981; Ager & Wallace, 1970; Wincierz 1973; Farrow, 1966; Seilacher, 1967). The conclusion is that the muddy facies was not intertidal but originated in somewhat deeper water than the respective ironstone facies.

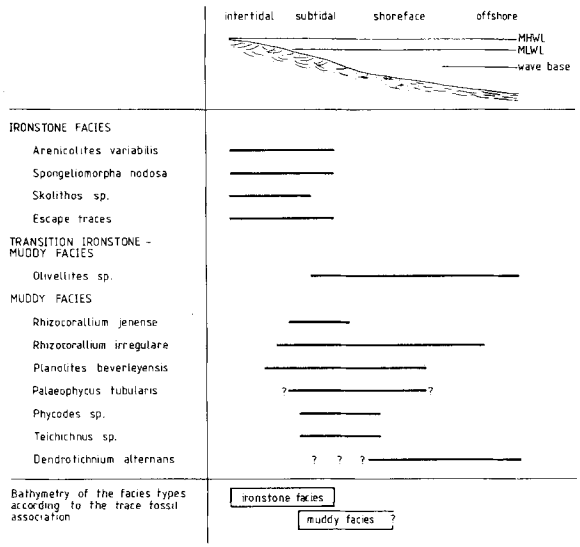


**Fig. 11.** Bathymetry of the facies types according to the ichnofaunal associations, bathymetric range of the traces after different sources (cf. text, also Teyssen, 1983a).

Secondly, wave ripple marks were investigated. Generally the effects of waves are less strong in the Minette than the effects of currents. But wave ripple marks can be found in both the muddy facies and the ironstone facies. They can be distinguished from current ripples by their symmetry and by additional diagnostic features of their internal structures (de Raaf, Boersma & van Gelder, 1977). Wave ripple marks were measured and used to estimate the parameters of the formative waves using a method of P. Allen (1981) (cf. also Homewood & Allen, 1981; Allen & Homewood, 1984; Komar, 1974; Allen, 1979; Miller & Komar, 1980). Conclusions from a bimodal distribution of wave periods led to the result of somewhat greater water depth for the muddy facies than for the ironstone facies, a general water depth between several metres and some ten metres seemed to be most probable (Teyssen, 1983a). The muddy facies should have formed seaward in front of subtidal shoals, the shoals prograding over a more distal muddy facies (cf. Siehl & Thein, 1978; van Houten & Bhattacharyya, 1982).

In principle there should not be any difference between migration of large-scale sand waves and advance of subtidal shoals over its distal muddy facies. Referring to and expanding the model of sand wave internal structure (Fig. 8) one should expect that in the case of exactly equal strengths of ebb and flood currents (not included in Fig. 8), a sand wave type will be developed which cannot be distinguished from a shoal. Subtidal shoals advancing over a distal muddy facies could in principle be incorporated into the sand wave conception of Fig. 8, but, practically, could not be recognized as sand waves in the field.

Upbuilding of the sedimentary record occurred as follows. It is not necessary to correlate regressions and transgressions with each individual cycle. Generally the lower part of the formation was built up by large-scale, subtidal sand waves overriding each other during progradation of the shoreline (general regression). On the other hand, there were transgressive events during deposition of the Minette as can be seen from the facies alterations in the upper part of the

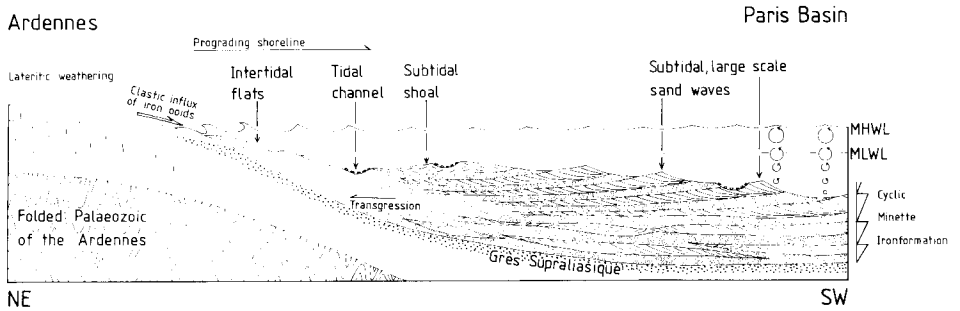


**Fig. 12.** Schematic section of the Minette depositional basin showing cyclic upbuilding of the formation, not to scale. Muddy facies dotted, ironstone facies white. See text for further explanation.

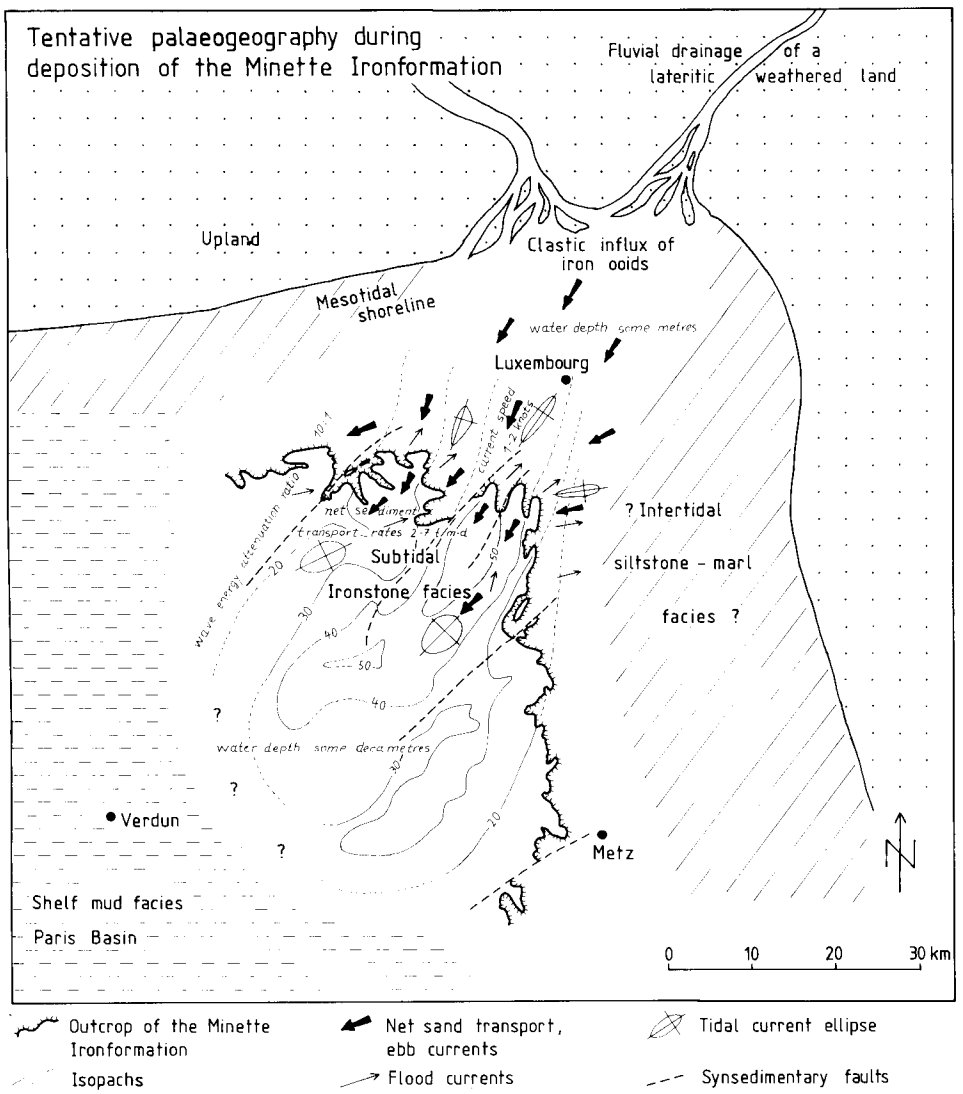


**Fig. 13.** Tentative palaeogeography during deposition to the Minette Iron Formation. Lateritic weathering on land and clastic influx of iron ooids after Siehl & Thein (1978), isopachs after IRSID (1967). Explanation in text.

sequence. There are hints at a shallowing of water depth (Achilles & Schulz, 1980; Teyssen, 1983a). Subtidal shoals were formed instead of sand waves. The shoals also migrated to the SW and gave rise to a similar cyclic development of the formation. Both large-scale sand waves and subtidal shoals were cut by tidal channels (cf. Fig. 5) within which medium-scale sand waves developed under channelized flow. The formation was built up in the frame of a progradation being disturbed by a few minor transgressive events (Fig. 12).

The ideas of Siehl & Thein (1978) on the genesis of the iron ooids themselves (which has not been the scope of this study) have been incorporated into the model depicted in Figs 12 and 13. The majority of the iron ooids may have been derived from latosols of continental areas under lateritic weathering, as has been concluded from geochemical investigations. That is also in accordance with the fact that most ooid cores are quartz grains or fragments of ooids or iron crusts and cores of fragments of carbonate shells are rare. The sedimentary structures give hints to turbulent, oxygen-rich water, which is in contradiction to Bubenicek's (1971) assumption of marine iron ooid genesis. Thus the ooids are supposed to have been formed on land and transported by rivers to the marine zone of accumulation.

A palaeogeographic map of the zone of Minette deposition (Fig. 13) summarizes most of the results which were obtained in the study of sand wave internal structures and in the analysis of wave ripple marks (Teyssen, 1983a). The lateral equivalents of the Minette in the more central part of the Paris Basin (cf. Megnien, 1980) are interpreted as shelf muds with respect to the overall palaeogeographical situation (cf. Ziegler, 1982). The position of the shoreline and of the intertidal zones (Fig. 13) is hypothetical, since recent erosion makes direct observations impossible.

There are some iron formations which are very similar to the Minette, and which have many sedimentological attributes that may be explained by the model proposed for the Minette (van Houten & Karasek, 1981; Bhattacharyya, 1980; Kimberley, 1980). But possible applications of the model presented above to other Iron Formations remain for the future.

## ACKNOWLEDGMENTS

This study is based on a Ph.D. thesis at Bonn university, supervised by Professor Siehl. I thank J. Bintz and the Geological Survey of Luxembourg for financial support for the field work. A grant of the 'Studienstiftung des deutschen Volkes' is gratefully acknowledged. I also thank D. Nio and the Comparative Sedimentology Division of the State University of Utrecht for the opportunity to study tidal sediments in The Netherlands. I thank T. de Mowbray and R. Visser (Utrecht) for guidance on the Oosterschelde sand wave deposits and interesting discussions. I owe special thanks to P. Homewood (Fribourg) for very fruitful discussions and hints during a joint field trip. F. B. van Houten (Princeton) and P. Homewood kindly read and improved an early draft of the manuscript. Last but not least I thank the reviewers, Ph. Allen and M. Talbot, for suggestions and criticisms which have improved the paper.

## REFERENCES

ACHILLES, H. & SCHULZ, H.-J. (1980) Geologische Untersuchungen in der Minette des Escher Beckens (Luxemburg). *Revue tech. luxemb.* 1980, pp. 93–141.

AGER, D.V. & WALLACE, P. (1970) The distribution of trace fossils in the uppermost Jurassic rocks of the Boulonnais, Northern France. In: *Trace Fossils* (Ed. by T. P. Crimes and J. C. Harper). *Geol. J. Spec. Issue No.* 3, pp. 1–18.

ALLEN, J.R.L. (1979) A model for the interpretation of wave ripple-marks using their wavelength, textural composition, and shape. *J. geol. Soc. London*, **136**, 673–682.

ALLEN, J.R.L. (1980) Sand waves: a model of origin and internal structure. *Sedim. Geol.* **26**, 281–328.

ALLEN, J.R.L. (1982) Mud drapes in sand wave deposits: a physical model with application to the Folkestone Beds (Early Cretaceous, southeast England). *Phil. Trans. R. Soc. A*, **306**, 291–345.

ALLEN, P.A. (1981) Some guidelines in reconstructing ancient sea conditions from wave ripple marks. *Mar. Geol.* **43**, M59–M67.

ALLEN, P.A. & HOMEWOOD, P. (1984) Evolution and mechanics of a Miocene tidal sandwave. *Sedimentology*, **31**, 63–81.

BHATTACHARYYA, D. (1980) *Sedimentology of the Late Cretaceous Nubia Formation at Aswan, southeast Egypt, and origin of the associated ironstones.* Ph.D. Thesis. Princeton University. 122 pp.

BOERSMA, J.R. (1969) Internal structure of some tidal megaripples on a shoal in the Westerschelde estuary, The Netherlands, report of a preliminary investigation. *Geologie Mijnb.* **48**, 409–414.

BOERSMA, J.R. & TERWINDT, J.H.J. (1981) Neap-spring tide sequences of intertidal shoal deposits in a mesotidal estuary. *Sedimentology*, **28**, 151–170.

BRAUN, H. (1964) Zur Entstehung der marin-sedimentären Eisenerze. *Clausthaler H. Lagerstättenk. Geochem. min. Rohst.* **2**, 133 pp.

BRINDLEY, G.W., BAILEY, S.W., FAUST, G.T., FORMAN, S.A. & RICH, C.I. (1968) Report of the nomenclature committee (66–67) of the Clay Minerals Society. *Clays Clay Miner.* **16**, 322–324.

BUBENICEK, L. (1964) Etude sédimentologique du minerais de fer oolithique de Lorraine. In: *Sedimentology and Ore Genesis* (Ed. by C. G. Amstutz, *Developments in Sedimentology*, **2**, 113–122. Elsevier, Amsterdam.

BUBENICEK, L. (1971) Géologie du gisement de fer de Lorraine. *Bull. Cent. Rech. Pau*, **5**, 223–320.

BUBENICEK, L. (1983) Diagenesis of iron-rich rocks. In: *Diagenesis in Sediments and Sedimentary Rocks*, 2 (Ed. by G. Larsen and G. V. Chilingar). *Developments in Sedimentology*, **25B**, 495–511, Elsevier, Amsterdam.

CAYEUX, L. (1922) *Les minerais de fer oolithiques de France*, fasc. II *Minerais de fer secondaires*. Ministère des Travaux publics, Paris, Imprimerie National.

DIMROTH, E. (1977) Facies models 5. Models of physical sedimentation of iron formations. *Geosci. Can.* **4**, 23–30.

FARROW, G.E. (1966) Bathymetric zonation of Jurassic trace fossils from the coast of Yorkshire, England. *Palaeogeogr. Palaeoclim. Palaeoecol.* **2**, 103–151.

FOX, W.T. (1967) FORTRAN IV program for vector trend analysis of directional data. *Comp. Contr. Kans. geol. Surv.* **11**, 1–36.

FÜRSICH, F.T. (1974) Corallian (Upper Jurassic) trace fossils from England and Normandy. *Stuttg. Beitr. Naturk. B, no.* 13, 52 pp.

FÜRSICH, F.T. (1975) Trace fossils as environmental indicators in the Corallian of England and Normandy. *Lethaia*, **8**, 151–172.

FÜRSICH, F.T. (1976) Fauna-substrate relationship in the Corallian of England and Normandy. *Lethaia*, **9**, 343–356.

FÜRSICH, F.T. (1977) Corallian (Upper Jurassic) marine benthic associations from England and Normandy. *Palaeontology*, **20**, 337–385.

FÜRSICH, F.T. (1981) Invertebrate trace fossils from the Upper Jurassic of Portugal. *Comm. Serv. Geol. Portugal*, **67**, 153–168.

HALLAM, A. (1966) Depositional environment of British Liassic ironstones considered in the context of their facies relationship. *Nature*, **209**, 1306–1307.

HALLAM, A. & BRADSHAW, M.J. (1979) Bituminous shales and oolitic ironstones as indicators of transgressions and regressions. *J. geol. Soc. London*, **136**, 157–164.

HALLIMOND, A.F. (1951) Problems of sedimentary iron ores. *Proc. Yorks. geol. Soc.* **28**, 61–66.

HAMMOND, F.D.C. & HEATHERSHAW, A.D. (1981) A wave theory for sand waves in shelf-seas. *Nature*, **293**, 208–210.

HEATH, R.A. (1981) Tidal asymmetry on the New Zealand coast and its implications for the net transport of sediment. *N. Z. J. Geophys.* **24**, 361–372.

HOMEWOOD, P. & ALLEN, P.A. (1981) Wave-, tide-, and current-controlled sandbodies of Miocene Molasse, western Switzerland. *Bull. Am. Ass. Petrol. Geol.* **65**, 2534–2545.

HOUBOLT, J.J.H.C. (1968) Recent sediments in the southern bight of the North Sea. *Geologie Mijnb.* **47**, 245–273.

HOUTEN, F.B. VAN & KARASEK, R.M. (1981) Sedimentologic framework of Late Devonian oolitic iron formations, Shatti valley, West-Central Libya. *J. sedim. Petrol.* **51**, 415–427.

HOUTEN, F.B. VAN & BHATTACHARYYA, D.P. (1982) Phanerozoic oolitic ironstones—geologic record and facies model. *Ann. Rev. Earth planet. Sci.* **10**, 441–457.

IRSID (1967) *Atlas géologique du gisement de fer de Lorraine*. Institut de recherche de la siderurgie, Mezaires-les-Metz, 23 maps.

JAMES, H.E. & HOUTEN, F.B. VAN (1979) Miocene goethitic and chamositic oolites, northeastern Colombia. *Sedimentology*, **26**, 125–133.

KENYON, N.H., BELDERSON, R.H., STRIDE, A.H. & JOHNSON, M.A. (1981) Offshore tidal sand-banks as indicators of net sand transport and as potential deposits. In: *Holocene Marine Sedimentation in the North Sea Basin* (Ed. by S.-D. Nio, R. T. E. Shüttenhelm and Tj. C. E. van Weering). *Spec. Publs int. Ass. Sediment.* **5**, 257–268. Blackwell Scientific Publications, Oxford.

KIMBERLEY, M. (1979) Geochemical distinctions among environmental types of iron formations. *Chem. Geol.* **25**, 185–212.

KIMBERLEY, M. (1980) The Paz de Rio oolitic inland-sea iron formation. *Econ. Geol.* **75**, 97–106.

KLEIN, G. DE VRIES, PARK, Y.A., CHANG, J.H. & KIM, C.S. (1982) Sedimentology of a subtidal, tide-dominated sand body in the Yellow Sea, southwest Korea. *Mar. Geol.* **50**, 221–240.

KOMAR, P.D. (1974) Oscillatory ripple marks and the evaluation of ancient wave conditions and environments. *J. sedim. Petrol.* **44**, 169–180.

LANGHORNE, D.N. (1982) A study of the dynamics of a marine sand wave. *Sedimentology*, **29**, 571–594.

LUCIUS, M. (1945) Die luxemburger Minetteformation und die jüngeren Eisenerzbildungen unseres Landes. Beiträge zur Geologie von Luxemburg. *Publs Serv. Carte géol. Luxemb.* **4**, 350 pp.

MEGNIEN, C. (Ed.) (1980) *Synthèse géologique du bassin de Paris*. vol. I Stratigraphie et paléogeographie, vol. II Atlas. *Mém. Bur. Rech. Géol. Min.* no. 101, 450 pp., no. 102, atlas, 60 maps.

MILLER, M.C. & KOMAR, P.D. (1980) A field investigation of the relationship between oscillation ripple spacing and their near-bottom water orbital motions. *J. sedim. Petrol.* **50**, 183–191.

MILLOT, G. (1970) *Geology of Clays—Weathering, Sedimentology, Geochemistry*. Springer-Verlag, New York. 425 pp.

MOWBRAY, T. DE & VISSER, M.J. (1982) Subordinate current reactivation surfaces and the recognition of tidal deposits. *Abstr. int. Ass. Sediment. 3rd Eur. mtg, Copenhagen*, 52–54.

NIO, S.-D. (1976) Marine transgressions as a factor in the formation of sandwave complexes. *Geologie Mijnb.* **55**, 18–40.

ODIN, G.S. & MATTER, A. (1981) De glauconiarum origine. *Sedimentology*, **28**, 611–641.

ORCEL, J., HÉNIN, S. & CAILLÈRE, S. (1949) Sur les silicates phylliteux de minerais de fer oolitique. *C. hebd. Séane. Acad. Sci. Fr.* **229**, 134–135.

RAAF, J.F.M. DE, BOERSMA, J.R. & GELDER, A. VAN (1977) Wave-generated structures and sequences from a shallow marine succession, Lower Carboniferous, County Cork, Ireland. *Sedimentology*, **24**, 451–483.

REINECK, H.E. (1963) Sedimentgefüge im Bereich der südlichen Nordsee. *Abh. senckenb. naturforsch. Ges.* **505**, 138 pp.

SEILACHER, A. (1967) Bathymetry of trace fossils. *Mar. Geol.* **5**, 413–428.

SHAKESBY, R.A. (1981) The application of trend surface analysis to directional data. *Geol. Mag.* **118**, 39–48.

SIEHL, A. & THEIN, J. (1978) Geochemische Trends in der Minette (Jura, Luxemburg/Lothringen). *Geol. Rdsch.* **67**, 1052–1077.

TAYLOR, J.H. (1949) Petrology of the Northampton Sand ironstone formation. *Mem. geol. Surv. U.K.*, 111 pp.

TEYSSEN, T. (1983a) *Gezeitenbeeinflußte Sedimentation und Sandwellenentwicklung in der Minette (Toarcium/Aalenium, Luxemburg/Lothringen)*. Ph.D. Thesis. Bonn University. 180 pp.

TEYSSEN, T. (1983b) Tide-controlled sedimentation and sand wave evolution in the Liassic Minette iron formation of Luxembourg and NE France. *Int. Ass. Sediment. 4th Reg. Mtg Split, Abstr.* pp. 166–169.

TEYSSEN, T. (1984) Physical model and FORTRAN IV program to estimate paleotidal flow velocities from features of sand waves. *Comput. Geosci. (in press).*

THEIN, J. (1975) Sedimentologisch-stratigraphische Untersuchungen in der Minette des Differdinger Beckens (Luxemburg). *Publs. Serv. Carte. géol. Luxemb.* **24**, 60 pp.

VISSER, M.J. (1980) Neap-spring cycles reflected in Holocene subtidal large-scale bedform deposits: a preliminary note. *Geology*, **8**, 543–546.

VISSER, M.J. & DE BOER, P. (1982) The effect of the diurnal inequality on tidal sediments: a tool in the recognition of tidal influences. *Int. Ass. Sediment. 3rd Eur. Mtg Copenhagen, Abstr.* pp. 88–90.

WINCIERZ, J. (1973) Küstensedimente und Ichnofauna aus dem oberen Hettangium von Mackendorf (Niedersachsen). *Neues Jb. Geol. Paläont. Abh.* **144**, 104–141.

ZIEGLER, P.A. (1982) *Geological Atlas of Western and Central Europe*. Elsevier, Amsterdam. 130 pp., 40 maps.

*(Manuscript received 17 June 1983; revision received 12 September 1983)*